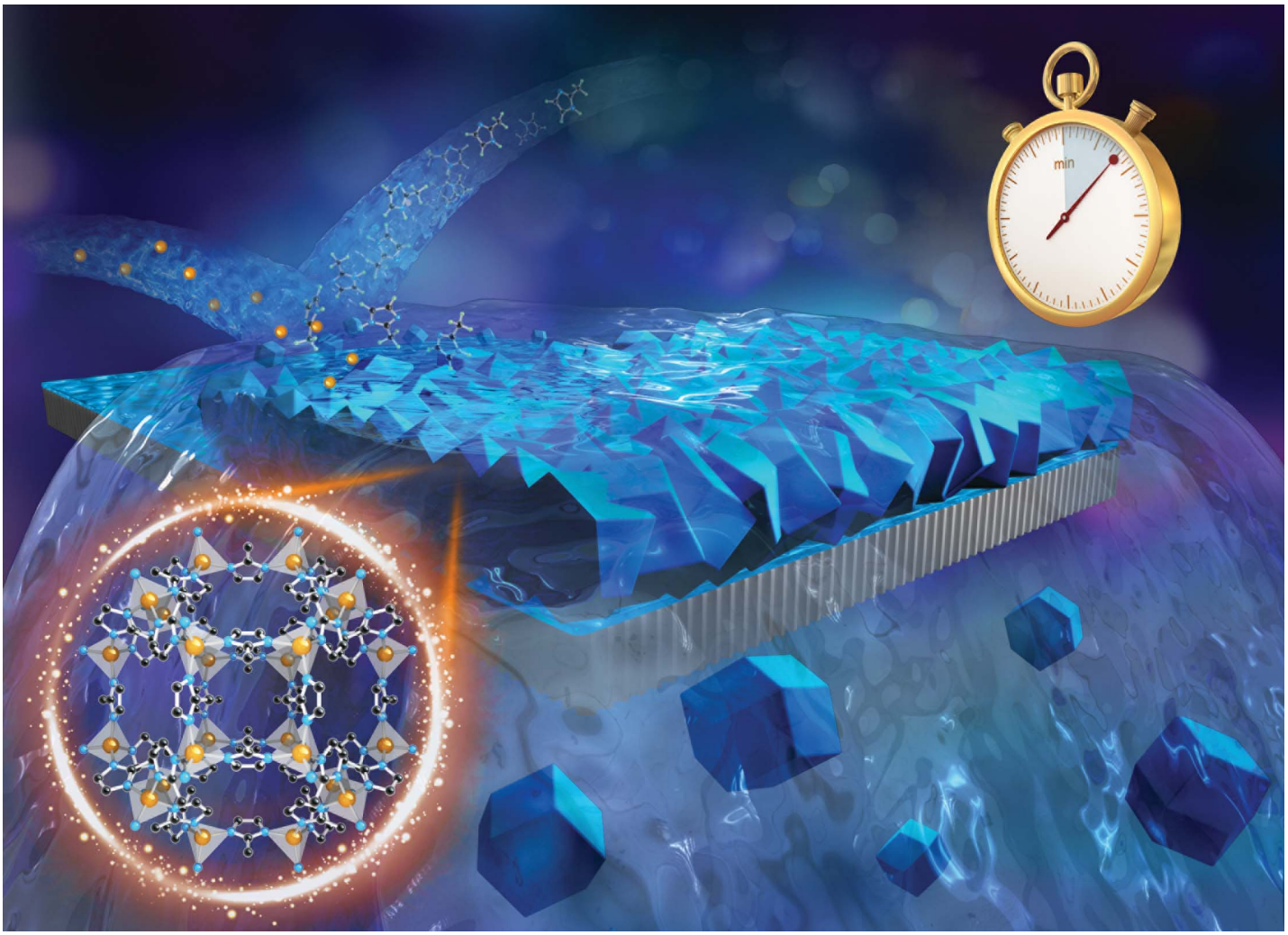

Showcasing a study on scalable crystallization of gas-sieving polycrystalline MOF films from Prof. Kumar Varoon Agrawal's laboratory, Institute of Chemical Sciences & Engineering (ISIC), École Polytechnique Fédérale de Lausanne (EPFL), Switzerland.

Synthesis of high-performance polycrystalline metal–organic framework membranes at room temperature in a few minutes

A route for rapid synthesis of high-performance metal-organic framework (MOF) membranes is reported. The crystallization is designed to maintain a high precursor concentration around the growing nuclei, allowing for uniform growth of MOF grains while hindering the Ostwald ripening. Well-intergrown polycrystalline MOF membranes with attractive gas separation performance could be obtained at room temperature in just 8 minutes, paving the way for the scale-up of polycrystalline MOF membranes.

As featured in:

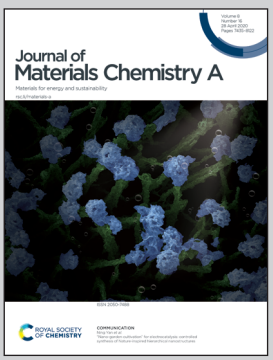

See Deepu J. Babu, Kumar Varoon Agrawal *et al.*, *J. Mater. Chem. A*, 2020, **8**, 7633.

ROYAL SOCIETY OF CHEMISTRY

rsc.li/materials-a

Registered charity number: 207890

Journal of Materials Chemistry A

ROYAL SOCIETY OF CHEMISTRY

COMMUNICATION

View Article Online
View Journal | View Issue

Cite this: J. Mater. Chem. A, 2020, 8, 7633

Received 1st November 2019
Accepted 13th December 2019

DOI: 10.1039/c9ta12027k

rsc.li/materials-a

Synthesis of high-performance polycrystalline metal–organic framework membranes at room temperature in a few minutes†

Jian Hao,[ab] Deepu J. Babu, *[a] Qi Liu,[a] Heng-Yu Chi,[a] Chunxiang Lu,[b] Yaodong Liu[b] and Kumar Varoon Agrawal *[a]

The development of a rapid and reproducible crystallization route for the synthesis of polycrystalline metal–organic framework (MOF) films is attractive for the scalable production of nanoporous membranes on porous supports. Prior crystallization studies have primarily focused on heterogeneous nucleation, and consequently, the time-consuming growth step has been overlooked. Here, we report a crystallization using sustained precursors (CUSP) route that maintains a high precursor concentration in the growth step, hindering the undesired Ostwald ripening observed in the late stage of growth. As a result, well-intergrown polycrystalline MOF films hosting a uniform grain size and a thickness of a few hundred nanometers could be obtained at room temperature in just a few minutes. Attractive gas separation performance is obtained from ZIF-8 membranes grown in 8 min with H_2/C_3H_8 selectivity of 2433 and C_3H_6/C_3H_8 selectivity of 30. The versatility of this approach is demonstrated by synthesizing a ZIF-67 membrane, as well as for the first time, a sub-1 μm-thick continuously intergrown ZIF-90 membrane, also in a few minutes, yielding H_2/CH_4 and H_2/C_3H_6 selectivities of 19.2 and 107.1, respectively. Such advances are expected to bring the scalable production of the high-performance polycrystalline MOF membranes a step closer to reality.

Introduction

Zeolitic imidazolate frameworks (ZIFs) are a subclass of metal–organic frameworks (MOFs) that exhibit zeolitic topology and are characterized by relatively high thermal and chemical stability.[1–4] Owing to the facile and reproducible crystallization chemistry, ZIFs have been increasingly used in catalysis,[5–7] drug delivery,[8] sensors,[9] storage,[10,11] separations,[12,13] *etc.* In particular, several ZIFs host a pore aperture between 3 and 4 Å, making them attractive for gas separation membranes.[14,15] For example, ZIF-8 and ZIF-90 hosting a crystallographically determined pore aperture of 3.4 Å [1] and 3.5 Å,[16] respectively, and a lattice-flexibility-induced[17,18] effective aperture of approximately 4.0 Å and 5.0 Å, have been investigated for a number of separations including H_2/CH_4, CO_2/CH_4, CO_2/N_2, C_3H_6/C_3H_8, *etc.*[1,15,19–26] The superior performance of ZIFs in gas separation has propelled intensive efforts to synthesize well-intergrown polycrystalline submicron-thick ZIF films in a scalable way. Generally, a synthesis route that allows rapid and reproducible crystallization of thin, well-intergrown ZIF films is preferred. In this respect, the traditional solvothermal crystallization route is disadvantageous compared to recently reported vapor-phase crystallization routes,[27,28] as the synthesis time for high-quality membranes in the former case is often several hours or days. This is mainly because the crystallization in the solvothermal route (dipping a substrate in a solution containing growth precursor solution) is difficult to control with the precursor concentration dropping as a function of time. However, at the same time, the solvothermal crystallization is highly promising for morphology engineering (controlling grain-size, grain-orientation, *etc.*) of thin films for manipulating their performance.[29,30]

The solvothermal synthesis of a polycrystalline film on a substrate involves the following steps: (i) nucleation or seeding of crystals on the substrate, (ii) growth of nuclei/seeds, and (iii) grain intergrowth. For applying polycrystalline ZIF films for size-sieving, it is desirable to synthesize thin yet pinhole-free and well-intergrown films on a porous support.[31] Generally, continuous ZIF films can be synthesized by dipping the substrate in the precursor sol in a batch mode,[32] however, the thickness and uniformity of such films are difficult to control. In such cases, to avoid pinholes, one has to synthesize films that are several micrometers thick, sacrificing the molecular flux. Recently, by decoupling the nucleation and the growth stages, the synthesis of submicron pinhole-free ZIF-8 films has been reported.[15,20,27,33–39] The nucleation stage involves the generation and attachment of a high density of ZIF nuclei or seed crystals,

[a]Laboratory of Advanced Separations (LAS), École Polytechnique Fédérale de Lausanne (EPFL), Rue de l'Industrie 17, CH-1951 Sion, Switzerland. E-mail: kumar.agrawal@epfl.ch; deepu.babu@epfl.ch

[b]CAS Key Laboratory of Carbon Materials, Institute of Coal Chemistry, Chinese Academy of Sciences, 27 Taoyuan South Road, Taiyuan, 030001, China

† Electronic supplementary information (ESI) available: Experimental details, characterization of the precursor solution, supplementary SEM images and the performance of the films in this study. See DOI: 10.1039/c9ta12027k

for example by surface modifications,[40–43] microwave irradiation,[44,45] electrophoretic deposition,[22,23,46,47] *etc.* This is followed by the growth of nuclei/seeds to eliminate any intercrystallite gaps. However, compared to the nucleation step, the growth step has received little attention so far, and as a result, the solvothermal crystallization is time-consuming. A route that cuts down the growth time to a few minutes would improve the scalability of the solvothermal route.

The growth step typically involves an extended immersion of the seeded substrate in a precursor solution for several hours or days. While the crystallization takes place on the substrate, it also takes place in the bulk of the precursor solution. Specifically, in the case of ZIF-8, upon mixing the Zn salt and the 2-methylimidazole (HmIm), an instantaneous cluster formation takes place. The clusters rapidly (in few seconds) transform into crystalline nanoparticles as observed by *in situ* X-ray scattering,[48] and *in situ* electron microscopy studies.[49] Naturally, as the growth proceeds, the precursor concentration drops rapidly, slowing down the crystallization kinetics considerably. Under these depleted precursor conditions, the Ostwald ripening becomes a predominant growth mechanism.[48,50] Specifically, in the evolution of polycrystalline film, the larger grains continue to grow at the expense of smaller grains leading to a poor grain intergrowth and an associated increase in the overall thickness of the film.

We hypothesized that by sustaining the precursor concentration, the Ostwald ripening of the grains can be restricted. This can be achieved by continuously supplying precursors to the growth environment. For example, recently Okubo and co-workers carried out solvothermal crystallization of zeolites in a custom-made continuous flow setup.[51] Similar flow setups have been used to obtain monodisperse MOF powders.[52] Herein, we report a crystallization using sustained precursors (CUSP) approach, involving a continuous supply of growth precursors over a substrate and demonstrate the synthesis of ZIF-8 membranes at room temperature in just 8 min with superior performance. By sustaining the precursor concentration, the Ostwald ripening was effectively hindered leading to uniformly sized grains and improved intergrowth in a short time, confirmed by the gas transport studies with H_2/C_3H_8 selectivity of 2433 and C_3H_6/C_3H_8 selectivity of 30. The versatility of this approach is demonstrated by extending CUSP for the synthesis of ZIF-67 and hybrid ZIF-8/ZIF-67 membranes. Also, for the first time, a high-quality submicron-thick ZIF-90 membrane could be synthesized using an aqueous precursor solution by the CUSP approach.

Results and discussion

The CUSP approach

We start by depositing a 100-nm-thick ZIF-8 seed layer on a porous anodic aluminum oxide (AAO) support using the electrophoretic nuclei assembly technique (Fig. S1†).[22,23] To pursue the film growth, the seed layer is typically immersed in a precursor solution in a batch mode. However, to obtain a well-intergrown pinhole-free film especially on a porous support, one needs to carry out the growth step for several hours.[22] Typically, during this period, the seed crystals evolve into non-uniform grains with micrometer-sized grains coexisting with smaller grains. An example of such growth is shown in Fig. 1a where the 100-nm-thick ZIF-8 seed layer is subjected to growth for 10 h at room temperature. The average grain density is approximately 3 grains per μm^2. The observed non-uniformity in the grain size has its roots in the Ostwald ripening, promoted by the depletion of the precursors (Zn^{2+} and HmIm), which in turn results from the simultaneous nucleation and growth of ZIF-8 in the precursor solution.

To understand the crystallization in the bulk of the precursor solution (homogeneous nucleation and growth), we tracked the evolution of crystals in solution using dynamic light scattering (DLS). The crystal-size-distribution evolved from a monomodal distribution in the initial growth stage (10 min of growth, mean size of 30 nm) to a bimodal distribution (centered at 30 and 550 nm) in 30 min of growth (Fig. S2†). At long growth time (1 h), the bimodal distribution (centered around 30 and 1829 nm) became dominated by micron-sized particles. The presence of nanometer-sized crystals at the later stage of growth indicates that nucleation continued even at 1 h. However, the initial rapid growth that led to 550 nm particles in 30 min slowed down significantly at the later stage. This is in accordance with the

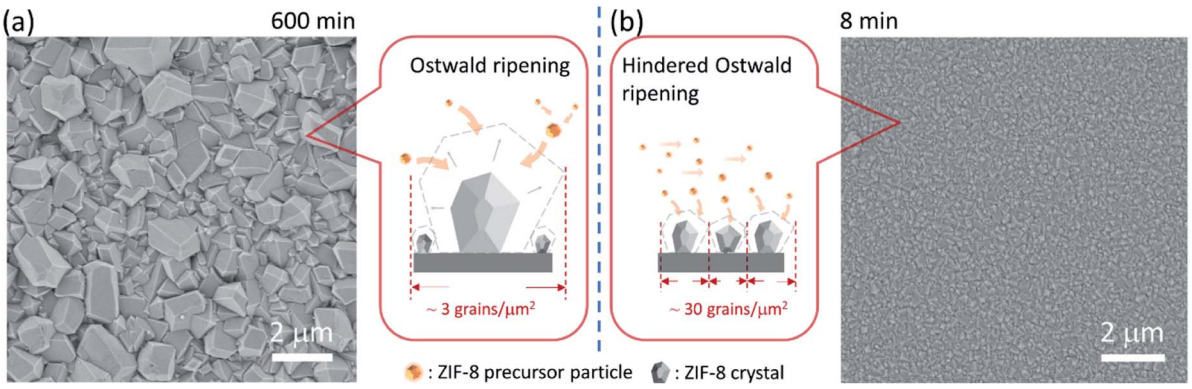

Fig. 1 Scanning electron microscopy (SEM) images of the ZIF-8 films and schematic illustrations of the corresponding growth mechanism. (a) ZIF-8 films grown by soaking nuclei film in precursor solution for 10 h, and (b) ZIF-8 film by the CUSP route with a growth time of 8 min.

typical growth stages observed for ZIF-8, *i.e.* a fast crystallization at first followed by a slower growth through the Ostwald-ripening in the precursor depleted growth solution.[48] The depletion of the deprotonated HmIm in the precursor solution was tracked by monitoring the pH of the growth solution. Indeed, the pH which was initially above 9.5, decreased continuously with time, dropping to 9.1 after 6 h of growth (Fig. S3†).

The CUSP approach circumvents the decrease in precursor concentration, observed above for the crystallization in batch mode. As a result, the CUSP process yields a well-intergrown ZIF-8 film hosting a uniform grain size (Fig. 1b). This approach addresses two rate-limiting steps of the crystal growth. First, the depletion of the precursors is avoided by continuously withdrawing and mixing/aging the precursors from their respective reservoirs (Fig. 2a). Second, the precursor solution is spread over the seeded substrate with low residence time. This ensures that most of the precursor solution contacts the growing film and that the precursors are primarily consumed by the nuclei film. The combined effect of these two factors helps to maintain a high growth rate while avoiding the transition to the Ostwald ripening stage.

The setup of the CUSP process is as follows; the metal and the ligand precursor solutions are delivered at a constant rate using two peristaltic pumps to a mixing chamber (Fig. 2a). After a predetermined mixing period, which we refer to as the dwell time, the precursor solution is spread on top of a pre-seeded substrate (Fig. 2b and c). The substrate is kept inclined (*ca.* 36°) to achieve a small residence time of 2 s. In this way, the effects of the dwell and the growth time on the morphology of the resulting films were studied. Keeping the dwell time fixed at 1 min, the results of several growth times (10, 12, 15, and 20 min) are presented in Fig. 2d–i. Intergrown films could be obtained in 10 min, however, few pinholes are visible when using a 100 nm-sized AAO substrate. We attribute these pinholes to the defects in the nuclei film (Fig. 2c and S1†). The defects were eliminated by increasing the growth time to 12 min, and a well-intergrown ZIF-8 film is obtained (Fig. 2e). The average grain size, $\bar{d}$, is calculated using eqn (1):

$$\bar{d} = \sqrt{\frac{1}{\rho}} \quad (1)$$

where ρ is the grain density per unit area. Unlike the conventional growth (Fig. 1a), the grains were uniform in size with a mean size of 230 nm (Fig. 2e). Micron-sized grains were not

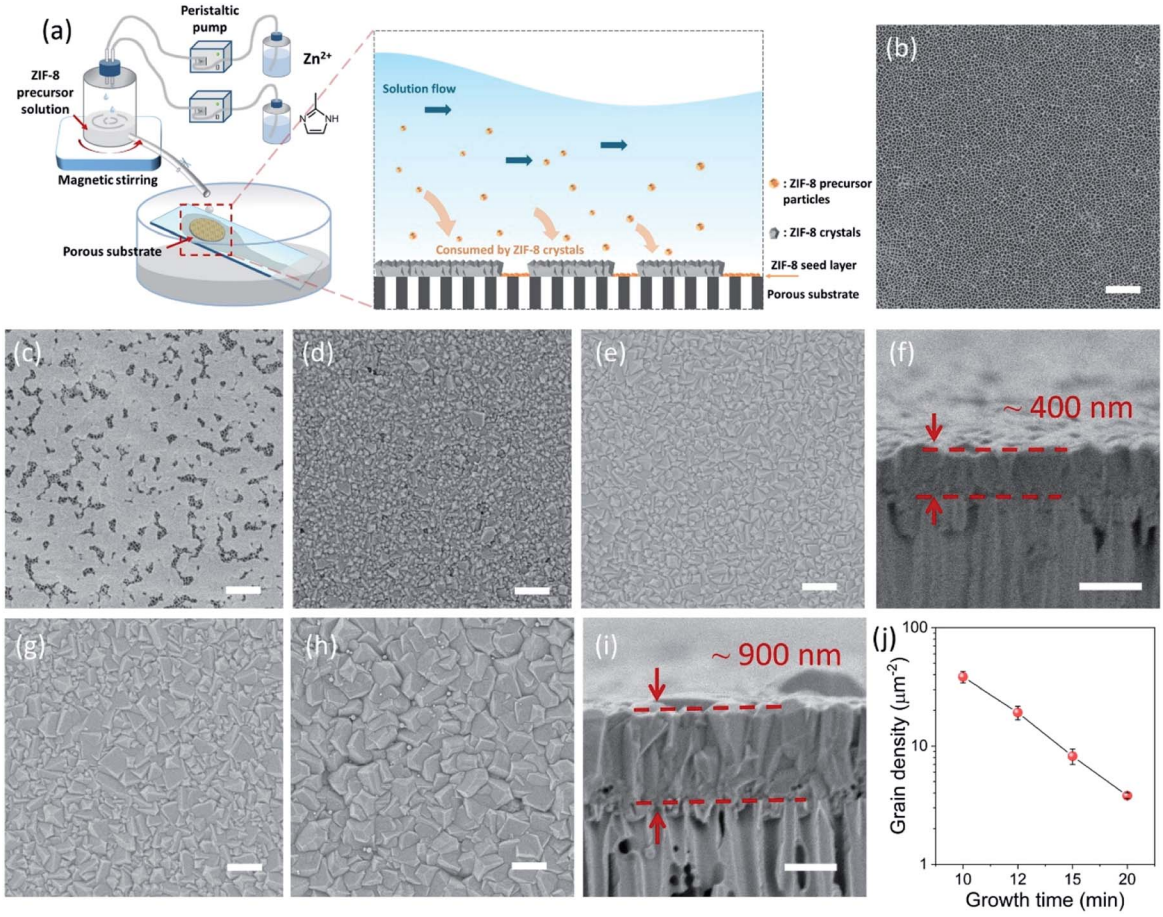

Fig. 2 (a) Schematic illustration of the CUSP setup. SEM images of (b) bare AAO hosting 100 nm-sized pores, (c) ZIF-8 nuclei film on AAO, and ZIF-8 films synthesized by the CUSP method for 10 min (d), 12 min (e and f), 15 min (g) and 20 min (h and i). (j) The ZIF-8 grain density as a function of the growth time. The scale bars represent 1 and 0.5 μm for top-view and cross-sectional-view panels, respectively.

observed. The pH of the precursor solution was sustained at 9.5 during the entire growth period (Fig. S3b†), which allowed a high growth rate. With further increase in growth time, grains continued to grow in size, increasing to 510 nm at 20 min of growth (Fig. 2h). The film thickness followed the increase in grain size and increased from 400 nm at 12 min (Fig. 2f) to about 900 nm at 20 min (Fig. 2i). The increase in grain size with the growth time is reflected by the decreasing grain density, from 38 grains per μm^2 at 10 min to less than 4 grains per μm^2 at 20 min of growth (Fig. 2j). A growth time of 12 min was sufficient to achieve good gas separation performance (discussed later). The grain density observed here, in 10–12 min of growth, is an order of magnitude larger than that reported in the literature.[55] The grains become relatively less uniform at longer growth time (Fig. 2g and h). This is because at longer time, the growth will primarily proceed on the top part of the intergrown grains exposed to the precursor solution. Since the film is not oriented, the exposed portion of the grain with varying facets tends to grow at different rates.[53,54] Therefore, growth time shorter than 12 min is optimal.

The morphology of the ZIF-8 film prepared by the CUSP approach was sensitive to the dwell time of precursors in the mixing chamber, and a shorter dwell time led to better intergrowth. No significant differences were observed for a dwell time in the range of 20 s to 2 min, and well-intergrown films were observed when grown for 12 min (Fig. 3a and b). However, when the dwell time was increased to 3 min, a complete intergrowth was observed only after 15 min (Fig. S4b†). To understand this, the concentration of HmIm was measured as a function of dwell time using UV-vis spectroscopy. An HmIm concentration above 0.50 mol L^{-1} was maintained at a dwell time below 2 min (Fig. 3c) with concentration decreasing slowly between 20 s and 2 min. Thereafter, a sharp decrease to 0.34 mol L^{-1} was observed when the dwell time was increased to 3 min. The corresponding DLS measurements indicate that ZIF-8 crystals in the precursor solution increased in size as a function of the dwell time. The full width at half maximum (FWHM) of the size-distribution also increased with the dwell time, from 31.3 nm at 20 s to 69.1 nm at 3 min (Fig. 3d). This can be attributed to the temporal overlap between the nucleation and growth phases.[50] The larger crystals in the solution are expected to increase the competition for the precursor solution, further slowing down the crystal growth. Hence, a dwell time smaller than 2 min was pursued.

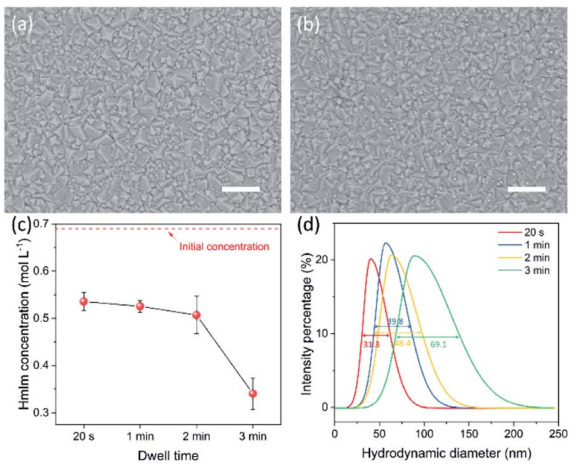

Fig. 3 SEM images of ZIF-8 films synthesized by 12 min of growth using dwell time of (a) 20 s and (b) 2 min. (c) The concentration of HmIm as a function of dwell time, and (d) the hydrodynamic diameter of ZIF-8 particles in the precursor solution at different dwell times. The scale bars are 1 μm.

The lower bound for the growth time to obtain a well-intergrown ZIF-8 film could be further reduced to 8 min (Fig. 1b) when using a porous support with a smaller pore size (20 nm). This is attributed to an improved nuclei film with fewer incidences of uncoated support surface (Fig. S5†) compared to that when a support with 100 nm pores was used (Fig. S1†). This is mainly because fewer nuclei (size of 10–20 nm)[22] are expected to infiltrate the 20 nm pores of the support. A short growth time of 8 min restricted the thickness of the intergrown film to 250 nm (Fig. S6†); yet these thin films yielded attractive separation performance (discussed in the next section). We emphasize that the growth time can be further reduced by optimizing the precursor mixing, and 8 min is not the limiting time. For example, we observed an increase in the crystallization kinetics by almost eliminating the dwell time by using a Y-configuration mixing instead of a separate mixing tank (Fig. S7a†). In this way, a well-intergrown ZIF-8 film could be obtained in 6 min (Fig. S7b†). The only caveat of this approach is that since the precursor flow is laminar, sufficient precaution should be taken to ensure proper mixing of the precursor solutions. Another possible route for further reducing the growth duration is by making use of the accelerated growth kinetics at an elevated temperature similar to what was demonstrated recently for the crystallization of the zeolite ZSM-5.[56]

Gas transport measurements

The gas transport measurements serve as a decisively indicative test for ascertaining the quality of a polycrystalline membrane. The single gas permeances as a function of the kinetic diameter of gases for the 8-min-grown ZIF-8 membrane, on a support hosting 20 nm pores, are shown in Fig. 4a. The membrane yielded an attractive H_2 permeance of 1.55×10^{-6} mol m^{-2} s^{-1} Pa^{-1} and an ideal H_2/CH_4 selectivity of 11.6 at room temperature, well above the corresponding Knudsen selectivity (2.8). As expected from a high-quality ZIF-8 membrane, the permeance of gases decreases as a function of the kinetic diameter (Fig. 4b). The H_2/C_3H_8 selectivity of 2433 and an attractive C_3H_6/C_3H_8 selectivity of 30.9 underscores the well-intergrown nature of the ZIF-8 membrane synthesized in just 8 min. Gas permeation measurements were also carried out on the ZIF-8 membrane synthesized on a support hosting 100 nm pores. These membranes also yielded attractive H_2 permeances in the range 1.0×10^{-6} to 2.1×10^{-6} mol m^{-2} s^{-1} Pa^{-1} with H_2 selectivity with respect to other gases increasing significantly as a function of the kinetic diameter (Fig. 4c and d). Data from four separate ZIF-8 membranes are reported in Table S1† confirming the highly reproducible nature of the CUSP method to synthesize high-quality ZIF-8 membranes.

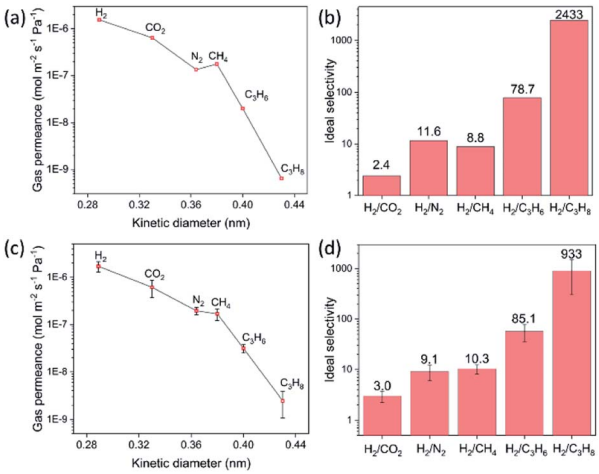

Fig. 4 Gas permeance from ZIF-8 membranes as a function of the kinetic diameter of gases at 25 °C. (a) Data from membranes grown in 8 min on an AAO support with a 20-nm-sized pore opening. (c) Average permeance data from membranes grown for 12, 15 and 20 min on AAO with a 100-nm-sized pore opening. The corresponding ideal selectivities of H_2 with respect to other gases are shown in (b) and (d), respectively.

The versatility of the CUSP approach

The CUSP approach allows one to synthesize well-intergrown MOF films, beyond the ZIF-8 framework, in a short time. For example, by changing the metal precursor to cobalt, a ZIF-67 film could be synthesized by the CUSP method (Fig. 5a and b). The reaction of HmIm with Co^{2+} is much faster than with Zn^{2+},[57] and therefore, the grain size in ZIF-67 film is larger than that in the ZIF-8 film when the synthesis time was 15 min. As a result, the thickness of the ZIF-67 film was 960 nm. We also extended the CUSP approach for the synthesis of hybrid membranes by simply switching the precursors. In this way, a hybrid ZIF-8/ZIF-67 membrane could be prepared (12 min growth for ZIF-8, and 8 min growth for ZIF-67; Fig. 5c and d). Attractive H_2 permeance and H_2/CH_4 selectivity from the ZIF-67 membrane (1.9×10^{-6} mol m^{-2} s^{-1} Pa^{-1} and 9.1, respectively) and hybrid ZIF-8/ZIF-67 membrane (2.3×10^{-6} mol m^{-2} s^{-1} Pa^{-1} and 9.3, respectively) confirm the versatility of the CUSP method for other MOF frameworks (Table S1†).

Furthermore, the CUSP approach could be used to synthesize highly intergrown sub-1-μm-thick ZIF-90 film. ZIF-90 is another stable nanoporous material in the ZIF family, and possesses a similar structure to that of ZIF-8, with 2-imidazolecarboxaldehyde (HIca) instead of HmIm linking the Zn nodes.[16] The carbonyl group of HIca makes ZIF-90 more hydrophilic and organophilic than ZIF-8.[18] The crystallization of sub-1 μm-thick ZIF-90 has proven to be challenging because the heterogeneous nucleation of ZIF-90 on a support surface is poor (Fig. S8†). Also, the ZIF-90 films are typically synthesized in dimethylformamide (DMF) or methanol as a solvent where films have a high tendency to develop cracks during the activation, *i.e.* removal of solvent (Fig. S9†). To the best of our knowledge, there are only a few reports on polycrystalline ZIF-90 membranes.[24,58] Except for one report, all ZIF-90 membranes were thicker than 5 μm. For example, Huang *et al.* reported about 20 μm-thick ZIF-90 membrane by covalent functionalization of the support followed by solvothermal synthesis at 100 °C for 18 h, yielding H_2 permeance of 2.5×10^{-7} mol m^{-2} s^{-1} Pa^{-1} and H_2/CH_4 selectivity of 15.2 at 200 °C.[24] Nair and coworkers reported a 5 μm-thick ZIF-90 membrane on seeded Torlon fiber by solvothermal synthesis at 65 °C for 4 h.[58] Recently, Jeong *et al.* applied a post-synthetic linker exchange approach to convert the top layer of ZIF-8 into ZIF-90.[45] However, the minimum time of effectively exchanging ZIF-8 to ZIF-90 was 2 days.

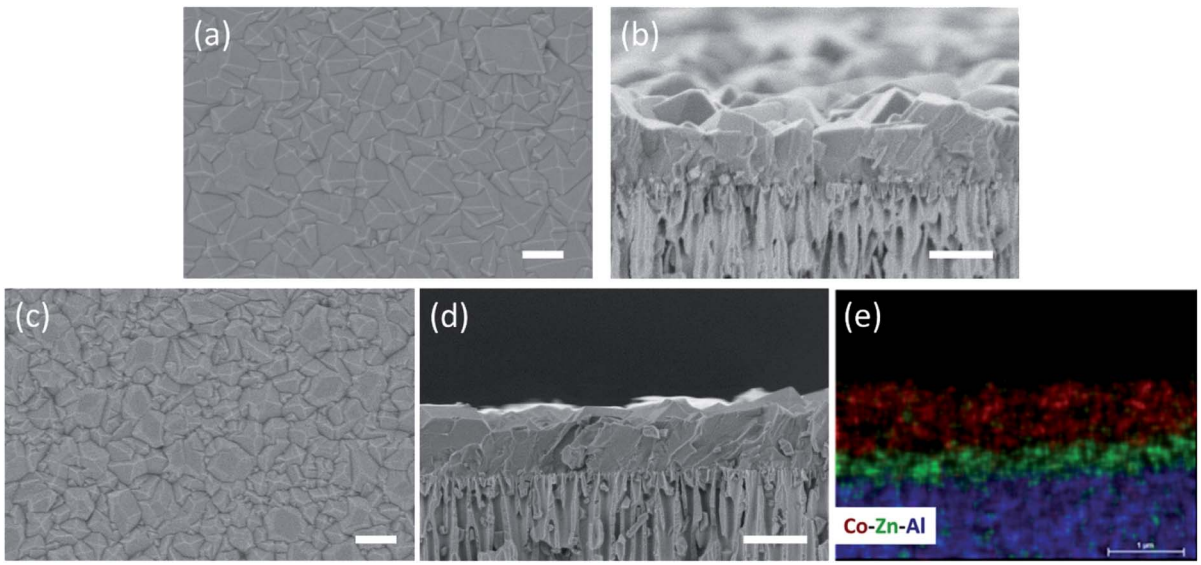

Fig. 5 SEM images of (a) ZIF-67 and (c) ZIF-8/ZIF-67. (b and d) are the corresponding cross-sectional views of films in (a) and (c), respectively. (e) The elemental mapping of the cross-sectional view of the film in (d). All scale bars correspond to 1 μm. In (e), red, green and blue correspond to Co, Zn and Al, respectively.

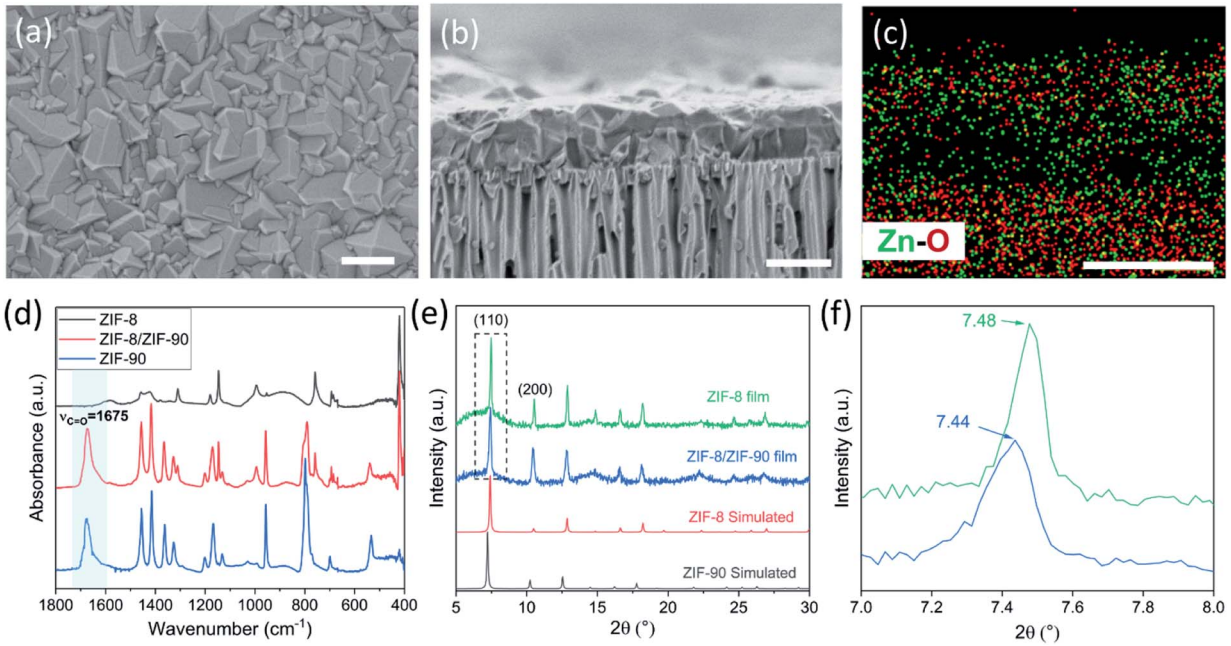

Fig. 6 SEM images of ZIF-8/ZIF-90 film: (a) top view, (b) cross-sectional view and (c) the corresponding elemental mapping. (d) FTIR plots of ZIF-8 film, ZIF-90 powder, and hybrid ZIF-8/ZIF-90 film. (e) XRD of ZIF-8 and hybrid ZIF-8/ZIF-90 films. (f) The enlarged XRD pattern showing the minor shift and broadening of the (110) peak in (e). All scale bars correspond to 1 μm.

In the CUSP approach, by switching the precursor solution for ZIF-8 to that for ZIF-90, aqueous-precursor-solution-based ZIF-90 films could be synthesized for the first time. This was also achieved in a relatively short time compared to the literature, *i.e.* 20 min at room temperature (Fig. 6a–c). Briefly, to increase the affinity of ZIF-90 crystals to the substrate, a defective layer of ZIF-8 was synthesized prior to the ZIF-90 growth where the ZIF-8 layer acts as a seed for the growth of ZIF-90 film (Fig. S10a and b†). The elemental analysis of the film cross-section clearly shows that the ZIF-90 film was crystallized on top of ZIF-8. The existence of ZIF-90 is further confirmed by FTIR wherein the ZIF-8/ZIF-90 film shows a characteristic carbonyl stretch at 1675 cm^{-1} (Fig. 6d). The X-ray diffraction (XRD) patterns (Fig. 6e) exhibit high crystallinity of the ZIF-8 layer as well as the hybrid ZIF-8/ZIF-90 film, while a minor shift and broadening of all peaks were observed for the hybrid film (Fig. 6f). The peak shifts are consistent with the simulated XRD patterns of ZIF-90 crystals.[1,16] The prepared hybrid ZIF-8/ZIF-90 membrane shows excellent H_2/CH_4 selectivity up to 19.2 and high H_2/C_3H_6 and C_3H_6/C_3H_8 selectivities of 107.1 and 10.7 respectively (Table S1†). It is noted that the underlying ZIF-8 layer of the composite film was intentionally made defective (Fig. S10a†). The high selectivities observed from the composite film confirm that the defects were fully covered by the ZIF-90 layer. Overall, the hybrid ZIF-90 membranes synthesized here performed better than ZIF-90 membranes in the literature (Table S2†).

Conclusions

Overall, we report a rapid yet versatile solvothermal crystallization approach for the synthesis of well-intergrown polycrystalline MOF membranes in a few minutes at room temperature. This was achieved by the CUSP approach which maintains the concentration of growth precursors, sustaining a high growth rate and hindering the Ostwald ripening. ZIF-8 membranes synthesized by the CUSP method in 8 min at room temperature exhibited similar performance to that of the state-of-the-art ZIF-8 membranes. We also demonstrated the versatility of this approach by synthesizing well-intergrown gas-sieving ZIF-67 and ZIF-90 membranes, making this approach highly attractive for the synthesis of MOF films.

Experimental section

Synthesis of ZIF-8 film

Two kinds of AAO substrates (pore opening: 20 nm and 100 nm respectively, diameter: 13 mm, Whatman), were used as substrates in this study. AAO substrates were sonicated in water for 20 min to remove surface contaminations. The ZIF-8 nuclei film on these substrates was prepared by the electrophoretic deposition method.[22,23]

For crystallization using the CUSP approach (Fig. 2a and S11†), two peristaltic pumps (PP1300, VWR) were used to continuously supply the precursor solutions into the mixing chamber. A valve was mounted on the downstream of the tube to control the flow rate of the solution flowing out. The flow rates of the zinc nitrate and the HmIm solutions were set at 2.0 and 2.3 mL min^{-1}, respectively. The precursors were introduced into a mixing chamber and stirred continuously. The "dwell time" was determined as the time from the first droplets entering into the chamber to the first droplet coming out of the chamber. After a predetermined dwell time, the downstream valve was opened to introduce the thoroughly mixed precursor

solution to the substrate coated with a nuclei film. The rate of outward flow from the mixing chamber was regulated to maintain the precursor solution at a constant level in the chamber. The downstream tube was positioned 1 cm above the upper side of the substrate and held in position by a clamp (Fig. S11†). The ZIF-8 precursor solution was added dropwise on the substrate which was held at an angle of *ca.* 36° and the duration of this process was determined as "growth time". After a certain growth time, the obtained ZIF-8 membrane was rinsed with deionized water and was allowed to dry at room temperature.

Synthesis of other ZIF films

The ZIF-67, the hybrid ZIF-8/ZIF-67, and the hybrid ZIF-8/ZIF-90 membranes were synthesized using a similar method to that used for the ZIF-8 membranes. The key differences are described below. For the ZIF-67 membrane, a cobalt nitrate solution was used as the metal precursor. For hybrid ZIF-8/ZIF-67 and ZIF-8/ZIF-90 films, a ZIF-8 film was synthesized at first. Then, for ZIF-67, the metal precursor was changed to the cobalt nitrate solution, and for ZIF-90, the ligand precursor was changed to the HIca solution. After rinsing the ZIF-8 film, a layer of ZIF-67 and ZIF-90 was directly synthesized on top of the ZIF-8 film.

Conflicts of interest

There are no conflicts to declare.

Acknowledgements

The authors acknowledge the home institution, EPFL, for generous support. A part of the project was funded by the Swiss National Science Foundation (SNSF) – Assistant Professor Energy Grant (PYAPP2_173645), and European Research Council (ERC) starting grant (805437-UltimateMembranes). J. H. acknowledges the scholarship from China Scholarship Council (CSC).

References

1 K. S. Park, Z. Ni, A. P. Cote, J. Y. Choi, R. Huang, F. J. Uribe-Romo, H. K. Chae, M. O'Keeffe and O. M. Yaghi, *Proc. Natl. Acad. Sci. U. S. A.*, 2006, **103**, 10186–10191.
2 R. Banerjee, A. Phan, B. Wang, C. Knobler, H. Furukawa, M. O'Keeffe and O. M. Yaghi, *Science*, 2008, **319**, 939–943.
3 J. Cravillon, S. Münzer, S.-J. Lohmeier, A. Feldhoff, K. Huber and M. Wiebcke, *Chem. Mater.*, 2009, **21**, 1410–1412.
4 B. Chen, Z. Yang, Y. Zhu and Y. Xia, *J. Mater. Chem. A*, 2014, **2**, 16811–16831.
5 C.-H. Kuo, Y. Tang, L.-Y. Chou, B. T. Sneed, C. N. Brodsky, Z. Zhao and C.-K. Tsung, *J. Am. Chem. Soc.*, 2012, **134**, 14345–14348.
6 O. Karagiaridi, M. B. Lalonde, W. Bury, A. A. Sarjeant, O. K. Farha and J. T. Hupp, *J. Am. Chem. Soc.*, 2012, **134**, 18790–18796.
7 X. Sun, A. I. O. Suarez, M. Meijerink, T. van Deelen, S. Ould-Chikh, J. Zečević, K. P. de Jong, F. Kapteijn and J. Gascon, *Nat. Commun.*, 2017, **8**, 1680.
8 C.-Y. Sun, C. Qin, X.-L. Wang, G.-S. Yang, K.-Z. Shao, Y.-Q. Lan, Z.-M. Su, P. Huang, C.-G. Wang and E.-B. Wang, *Dalton Trans.*, 2012, **41**, 6906–6909.
9 G. Lu and J. T. Hupp, *J. Am. Chem. Soc.*, 2010, **132**, 7832–7833.
10 Y. Peng, V. Krungleviciute, I. Eryazici, J. T. Hupp, O. K. Farha and T. Yildirim, *J. Am. Chem. Soc.*, 2013, **135**, 11887–11894.
11 H. Wu, W. Zhou and T. Yildirim, *J. Am. Chem. Soc.*, 2007, **129**, 5314–5315.
12 B. R. Pimentel, A. Parulkar, E. Zhou, N. A. Brunelli and R. P. Lively, *ChemSusChem*, 2014, **7**, 3202–3240.
13 K. Li, D. H. Olson, J. Seidel, T. J. Emge, H. Gong, H. Zeng and J. Li, *J. Am. Chem. Soc.*, 2009, **131**, 10368–10369.
14 Y. Li, F. Liang, H. Bux, A. Feldhoff, W. Yang and J. Caro, *Angew. Chem., Int. Ed.*, 2010, **49**, 548–551.
15 H. Bux, F. Liang, Y. Li, J. Cravillon, M. Wiebcke and J. Caro, *J. Am. Chem. Soc.*, 2009, **131**, 16000–16001.
16 W. Morris, C. J. Doonan, H. Furukawa, R. Banerjee and O. M. Yaghi, *J. Am. Chem. Soc.*, 2008, **130**, 12626–12627.
17 C. Zhang, R. P. Lively, K. Zhang, J. R. Johnson, O. Karvan and W. J. Koros, *J. Phys. Chem. Lett.*, 2012, **3**, 2130–2134.
18 K. Eum, K. C. Jayachandrababu, F. Rashidi, K. Zhang, J. Leisen, S. Graham, R. P. Lively, R. R. Chance, D. S. Sholl, C. W. Jones and S. Nair, *J. Am. Chem. Soc.*, 2015, **137**, 4191–4197.
19 D. J. Babu, G. He, J. Hao, M. T. Vahdat, P. A. Schouwink, M. Mensi and K. V. Agrawal, *Adv. Mater.*, 2019, **31**, 1900855.
20 H. T. Kwon and H. K. Jeong, *J. Am. Chem. Soc.*, 2013, **135**, 10763–10768.
21 H. T. Kwon, H. K. Jeong, A. S. Lee, H. S. An and J. S. Lee, *J. Am. Chem. Soc.*, 2015, **137**, 12304–12311.
22 G. He, M. Dakhchoune, J. Zhao, S. Huang and K. V. Agrawal, *Adv. Funct. Mater.*, 2018, **28**, 1707427.
23 G. He, D. J. Babu and K. V. Agrawal, *J. Visualized Exp.*, 2018, e58301.
24 A. Huang, W. Dou and J. Caro, *J. Am. Chem. Soc.*, 2010, **132**, 15562–15564.
25 A. Huang and J. Caro, *Angew. Chem., Int. Ed.*, 2011, **50**, 4979–4982.
26 A. Huang, N. Wang, C. Kong and J. Caro, *Angew. Chem., Int. Ed.*, 2012, **51**, 10551–10555.
27 X. Ma, P. Kumar, N. Mittal, A. Khlyustova, P. Daoutidis, K. A. Mkhoyan and M. Tsapatsis, *Science*, 2018, **361**, 1008–1011.
28 W. Li, P. Su, Z. Li, Z. Xu, F. Wang, H. Ou, J. Zhang, G. Zhang and E. Zeng, *Nat. Commun.*, 2017, **8**, 1–8.
29 Z. Lai, G. Bonilla, I. Diaz, J. G. Nery, K. Sujaoti, M. A. Amat, E. Kokkoli, O. Terasaki, R. W. Thompson, M. Tsapatsis and D. G. Vlachos, *Science*, 2003, **300**, 456–460.
30 Y. Li, H. Bux, A. Feldhoff, G. Li, W. Yang and J. Caro, *Adv. Mater.*, 2010, **22**, 3322–3326.
31 D. J. Babu, G. He, L. F. Villalobos and K. V. Agrawal, *ACS Sustainable Chem. Eng.*, 2019, **7**, 49–69.
32 H. Bux, A. Feldhoff, J. Cravillon, M. Wiebcke, Y. S. Li and J. Caro, *Chem. Mater.*, 2011, **23**, 2262–2269.

33 J. Yao, D. Dong, D. Li, L. He, G. Xu and H. Wang, *Chem. Commun.*, 2011, **47**, 2559–2561.
34 M. N. Shah, M. A. Gonzalez, M. C. McCarthy and H. K. Jeong, *Langmuir*, 2013, **29**, 7896–7902.
35 F. Cacho-Bailo, S. Catalán-Aguirre, M. Etxeberría-Benavides, O. Karvan, V. Sebastian, C. Téllez and J. Coronas, *J. Membr. Sci.*, 2015, **476**, 277–285.
36 Y. Hu, J. Wei, Y. Liang, H. Zhang, X. Zhang, W. Shen and H. Wang, *Angew. Chem., Int. Ed.*, 2016, **55**, 2048–2052.
37 E. Shamsaei, Z. X. Low, X. Lin, A. Mayahi, H. Liu, X. Zhang, J. Zhe Liu and H. Wang, *Chem. Commun.*, 2015, **51**, 11474–11477.
38 P. Yang, Z. Li, Z. Gao, M. Song, J. Zhou, Q. Fang, M. Xue and S. Qiu, *ACS Sustainable Chem. Eng.*, 2019, **7**, 4158–4164.
39 M. C. McCarthy, V. Varela-Guerrero, G. V. Barnett and H. K. Jeong, *Langmuir*, 2010, **26**, 14636–14641.
40 Q. Liu, N. Wang, J. Caro and A. Huang, *J. Am. Chem. Soc.*, 2013, **135**, 17679–17682.
41 N. Wang, Y. Liu, Z. Qiao, L. Diestel, J. Zhou, A. Huang and J. Caro, *J. Mater. Chem. A*, 2015, **3**, 4722–4728.
42 A. Huang, H. Bux, F. Steinbach and J. Caro, *Angew. Chem., Int. Ed.*, 2010, **49**, 4958–4961.
43 J. Hou, P. D. Sutrisna, Y. Zhang and V. Chen, *Angew. Chem., Int. Ed.*, 2016, **55**, 3947–3951.
44 H. T. Kwon and H. K. Jeong, *Chem. Commun.*, 2013, **49**, 3854–3856.
45 M. J. Lee, H. T. Kwon and H.-K. Jeong, *Angew. Chem., Int. Ed.*, 2018, **57**, 156–161.
46 L. Besra and M. Liu, *Prog. Mater. Sci.*, 2007, **52**, 1–61.
47 I. Hod, W. Bury, D. M. Karlin, P. Deria, C. W. Kung, M. J. Katz, M. So, B. Klahr, D. Jin, Y. W. Chung, T. W. Odom, O. K. Farha and J. T. Hupp, *Adv. Mater.*, 2014, **26**, 6295–6300.
48 J. Cravillon, C. A. Schröder, R. Nayuk, J. Gummel, K. Huber and M. Wiebcke, *Angew. Chem., Int. Ed.*, 2011, **50**, 8067–8071.
49 J. P. Patterson, P. Abellan, M. S. Denny, C. Park, N. D. Browning, S. M. Cohen, J. E. Evans and N. C. Gianneschi, *J. Am. Chem. Soc.*, 2015, **137**, 7322–7328.
50 M. J. Van Vleet, T. Weng, X. Li and J. R. Schmidt, *Chem. Rev.*, 2018, **118**, 3681–3721.
51 Z. Liu, T. Wakihara, K. Oshima, D. Nishioka, Y. Hotta, S. P. Elangovan, Y. Yanaba, T. Yoshikawa, W. Chaikittisilp, T. Matsuo, T. Takewaki and T. Okubo, *Angew. Chem., Int. Ed.*, 2015, **54**, 5683–5687.
52 X. G. Wang, Q. Cheng, Y. Yu and X. Z. Zhang, *Angew. Chem., Int. Ed.*, 2018, **57**, 7836–7840.
53 J. Troyano, A. Carné-Sánchez, C. Avci, I. Imaz and D. Maspoch, *Chem. Soc. Rev.*, 2019, **48**, 5534–5546.
54 Y. Pan, D. Heryadi, F. Zhou, L. Zhao, G. Lestari, H. Su and Z. Lai, *CrystEngComm*, 2011, **13**, 6937–6940.
55 S. Tanaka, K. Okubo, K. Kida, M. Sugita and T. Takewaki, *J. Membr. Sci.*, 2017, **544**, 306–311.
56 Z. Liu, K. Okabe, C. Anand, Y. Yonezawa, J. Zhu, H. Yamada, A. Endo, Y. Yanaba, T. Yoshikawa, K. Ohara, T. Okubo and T. Wakihara, *Proc. Natl. Acad. Sci. U. S. A.*, 2016, **113**, 14267–14271.
57 C. L. Hobday, T. D. Bennett, D. Fairen-Jimenez, A. J. Graham, C. A. Morrison, D. R. Allan, T. Düren and S. A. Moggach, *J. Am. Chem. Soc.*, 2018, **140**, 382–387.
58 A. J. Brown, J. R. Johnson, M. E. Lydon, W. J. Koros, C. W. Jones and S. Nair, *Angew. Chem., Int. Ed.*, 2012, **51**, 10615–10618.